Journal of Analytical and Applied Pyrolysis 183 (2024) 106821

Contents lists available at ScienceDirect

Journal of Analytical and Applied Pyrolysis

journal homepage: www.elsevier.com/locate/jaap

Differential hydrocarbon generation characteristics of organic matter with green algae and cyanobateria origins in the Permain Lucaogou Formation of the Santanghu Basin

Miao Yu [a,b], Gang Gao [a,b,*], Hui Liang [c], Miao Liu [a,b], Jilun Kang [c], Xiongfei Xu [c], Wei Zhang [c]

[a] College of Geosciences, China University of Petroleum, Beijing 102249, China
[b] National Key Laboratory of Petroleum Resources and Engineering, Beijing, 102249, China
[c] PetroChina Tuha Oilfield Company, Hami, 839009, China

ARTICLE INFO

Keywords:
Fine grained rock
Cyanobacteria
Green algae
Kinetics
Lucaogou formation

ABSTRACT

Organic-rich fine-grained rocks are key carriers of unconventional oil and gas resources, making it crucial to understand their hydrocarbon generation and evolution characteristics. This study examines the fine-grained rocks of the second member of the Lucaogou Formation (P_2l_2) in the Tiaohu and Malang Sags of the Santanghu Basin, focusing on how different organic matter (OM) backgrounds - primarily green algae and cyanobacteria - affect hydrocarbon generation and crude oil properties. Kinetic analysis and hydrous pyrolysis experiments on shales rich in green algae, cyanobacteria, and their mixtures revealed that green algae - derived OM requires lower activation energy to initiate hydrocarbon generation, results in an earlier oil generation peak, and has a broader oil window. Conversely, cyanobacteria - derived OM needs higher activation energy to start hydrocarbon generation, has a later oil peak, and a more concentrated generation period. These findings led to two models: the "green algae origin - early hydrocarbon generation - early oil peak - broad oil window model" and the "cyanobacteria origin - late hydrocarbon generation - late oil peak - concentrated oil generation model." Correlation analysis showed that aromatic hydrocarbons, resins, and asphaltenes significantly degrade crude oil quality. Hydrous pyrolysis experiments indicated that the heavy component content (aromatic hydrocarbons + resins + asphaltenes) in liquid hydrocarbons follows the order: residual oil > absorbed oil > expelled oil, with content initially increasing and then decreasing with maturity, and the color change of liquid hydrocarbons in dichloromethane reflects heavy component content changes effectively. Calculations of density and viscosity of liquid hydrocarbons, based on heavy component content and crude oil properties, were compared with the longitudinal distribution of crude oil properties in the study area. Results show that the hydrocarbon generation characteristics of green algae and cyanobacteria control crude oil properties, highlighting significant intra-source differentiation in the P_2l_2 shale and validates the phase separation approach in hydrous pyrolysis experiments. The P_2l_2 shale, with its high OM content and substantial hydrocarbon generation, holds great potential for shale oil exploration, but both reservoir quality and crude oil property evolution under different OM backgrounds should be considered when selecting favorable areas.

1. Introduction

Fine-grained rocks, characterized by significant thickness and abundant organic matter (OM), are widely distributed in sedimentary basins, making them important hosts for shale oil and tight oil in petroleum exploration and development [1–3]. The kinetic characteristics of hydrocarbon generation in organic-rich shales are crucial for determining optimal conditions for shale oil extraction [4–6]. Based mainly on the principle of temperature-time complementarity, many scholars conduct high-temperature, rapid pyrolysis experiments in the laboratory to evaluate hydrocarbon potential, pyrolysis mechanisms, and pore evolution characteristics of immature or low-maturity stage OM [7,8]. The heterogeneity of lacustrine fine-grained sedimentary source rocks results in significant variations in the deposition and

* Correspondence to: National Key Laboratory of Petroleum Resources and Engineering, College of Geosciences, China University of Petroleum, Beijing 102249, China.
E-mail address: gg_2819@163.com (G. Gao).

https://doi.org/10.1016/j.jaap.2024.106821
Received 27 June 2024; Received in revised form 23 September 2024; Accepted 14 October 2024
Available online 17 October 2024

preservation of OM across various sedimentary environments [9], leading to distinct hydrocarbon generation kinetics [10,11]. This difference is reflected not only in the activation energy between different types of kerogens but also in the kinetic parameters of hydrocarbon generation even within the same type of kerogen [6,7]. Generally, experimental systems for hydrocarbon generation kinetics analysis are classified into open, semi-open, and closed systems [12,13]. Among them, open and closed system thermal simulations are more commonly used due to their frequent application in studying kerogen decomposition and heavy hydrocarbon cracking processes [5,7,11].

Long-term oil and gas exploration has confirmed that OM such as spores, pollen, bacteria, algae, and higher plants play a significant role in the formation of hydrocarbons [14–16]. For instance, the OM in the Green River Shale in the United States is primarily composed of cyanobacteria and green algae [17], In Australia, the Rundle-type shale is mainly composed of Pediastrum from the Chlorophyceae family [18], while the Alberta Shale in Canada primarily consists of cyanobacteria [19]. Many scholars have conducted hydrocarbon generation kinetic analyses on organic-rich source rocks [20–22]. For example, Meng et al. [23] conducted hydrocarbon generation simulations on benthic algae, clarifying their bimodal hydrocarbon generation characteristics. Yu et al. [16,24] compared the hydrocarbon generation kinetics of lamalginite from two saline lakes in the Junggar Basin, providing a basis for further hydrocarbon source analysis in the region. Similarly, Liu et al. [25] compared the hydrocarbon generation characteristics of lamalginite and telalginite from the Lucaogou Formation in the Jimsar Sag of the Junggar Basin, offering new insights into the enrichment mechanisms of shale oil sweet spots. Furthermore, Li et al. [11] added modern spores and pollen to shale samples from the Bozhong Sag in the Bohai Bay Basin, successfully explained the bimodal hydrocarbon generation origin of OM in the research area.

In favorable conditions, some of the crude oil generated in source rocks can migrate and be expelled into reservoirs with better physical properties, forming conventional or tight oil reservoirs, while the remaining crude oil accumulates within the source rock itself, forming shale oil reservoirs [26]. However, most of the aforementioned hydrocarbon generation kinetic studies primarily simulate the quantity and expulsion of oil generated from OM, with relatively few studies focusing on the geochemical characteristics of the oil that influence its migration and in-situ accumulation, such as the physical properties of the crude oil [7,8,10]. For example, determining whether the density and viscosity of crude oil generated from different types of the OM vary at different stages of evolution is crucial for identifying shale oil enrichment areas and selecting “sweet spots” for shale oil development [27,28].

The second member of the Lucaogou Formation (P_2l_2) in the Santanghu Basin is characterized by the deposition of fine-grained sediments primarily derived from air-fall volcanic ash, with OM predominantly composed of cyanobacteria and green algae [29–32]. Previous studies suggest that volcanic activity influences climate conditions, which in turn affects the development of OM [31]. During volcanic eruption periods, the climate is relatively warm and humid, resulting in lower water salinity and a dominance of cyanobacteria. Conversely, during inter-eruption periods, higher water salinity favors the development of green algae or a mixture of cyanobacteria and green algae [29–32]. The primary aim of this study is to build on previous research regarding the mechanisms of OM enrichment in the P_2l_2, integrating hydrocarbon generation kinetics experiments and relevant geochemical analyses. The main objectives are to establish hydrocarbon generation models for OM primarily derived from cyanobacteria and green algae, determine the evolution patterns of hydrocarbon products from different organic sources, and provide insights for selecting “sweet spots” in shale oil exploration.

2. Regional geology

The Santanghu Basin is located in the northeastern of Xinjiang Province, China, extending in a northwest-southeast direction [33]. The western and southern parts of the basin are adjacent to the Junggar Basin and the Turpan-Hami Basin, respectively, covering an area of approximately 23,000 km^2 (Fig. 1a) [34,35]. The basin has undergone multiple phases of tectonic evolution, including the early Permian extensional fault depression-subsidence basin formation stage, the late Permian to early Triassic regional compression and transformation stage, the mid-late Triassic to Paleogene subsidence basin formation stage, and the Neogene compressional thrust-slip transformation and intermontane basin formation stage [36]. Currently, it can be divided into three primary structural units: the northern uplift belt, the southern thrust belt, and the central depression belt [37,38]. The central depression belt is divided into six sags and five uplifts (Fig. 1b) [39], with the study area primarily located in the Tiaohu and Malang Sags, covering a total area of approximately 3200 km^2, which is currently the most explored area of the basin [33,40,41].

The Santanghu Basin lacks both the Upper and Lower Permian, with only the Middle Permian remaining, which is unconformably in contact with the underlying Upper Carboniferous and the overlying Mesozoic strata [42,43]. Drilling reveals that the Middle Permian strata have a thickness exceeding 1000 m and exhibit a south-thickening, north--thinning characteristic, with the Lucaogou Formation and Tiaohu Formation deposited sequentially from oldest to newest (Fig. 1c) [44]. Drilling in the Lucaogou Formation reveals a thickness ranging from approximately 100 to 700 m, which can be vertically divided into three members based on electrical characteristics, from oldest to newest: member 1, member 2, and member 3 of the Lucaogou Formation (Fig. 1a) [45]. During the P_2l_2 depositional period, periodic volcanic activity around the basin led to the deposition of significant volcanic ash in the lake, resulting in a set of lacustrine fine-grained sediments dominated by volcanic materials and carbonate minerals [31,32,46]. The sediment thickness ranges from 150 to 300 m, with high OM content, making it an excellent source rock with various types of pores, and a primary target for current shale oil exploration [37].

3. Materials and methods

In this study, over 200 samples were collected from more than ten wells in the Tiaohu and Malang Sags of the Santanghu Basin for systematic organic petrology observations. The results indicate that the enrichment levels of cyanobacteria and green algae vary among different lithologies of fine-grained rocks, closely related to volcanic eruption cycles and paleoclimate conditions [32]. Based on analyses of total organic carbon (TOC), rock pyrolysis (Rock-Eval), vitrinite reflectance (Ro), and Scanning electron microscope (SEM), three samples with lower organic maturity were selected from well LY1 in the Malang Sag, with organic compositions predominantly consisting of cyanobacteria (sample LY1-a) (Fig. 2a and d; Table S1), green algae (sample LY1-b) (Fig. 2e and h), and a mix of cyanobacteria and green algae (sample LY1-c) (Fig. 2i and l). Notably, cyanobacteria are often associated with felsic minerals (Fig. 2b, c, j and k), while green algae remain well-developed even in environments with high carbonate mineral content (Fig. 2f, g, j and k). The TOC content of the three samples is 5.57 %, 3.66 %, and 3.87 %, respectively (Table S1), with Rock-Eval S_2 values of 40.20 mg/g, 17.39 mg/g, and 23.96 mg/g, and hydrogen index ($HI = S_2 \times 100/TOC$) of 722 mg/g TOC, 475 mg/g TOC, and 619 mg/g TOC, indicating high OM abundance and primarily Type I and Type II kerogen. Additionally, the Tmax and Ro values for all three samples are around 438℃ and 0.71 %, indicating low maturity (Table S1). Furthermore, kerogen was prepared from these samples for kerogen carbon isotope ($\delta^{13}C_{kerogen}$) analysis (Table S1), enhancing the rationale for sample selection. The $\delta^{13}C_{kerogen}$ values for samples LY1-a (cyanobacteria - origin), LY1-b (green algae - origin), and LY1-c (mixed origins of cyanobacteria and green algae) are −30.3 ‰, −25.7 ‰, and −27.9 ‰, respectively, indicating that the $\delta^{13}C_{kerogen}$ in the cyanobacteria-rich sample is lighter, in the green algae-rich sample is

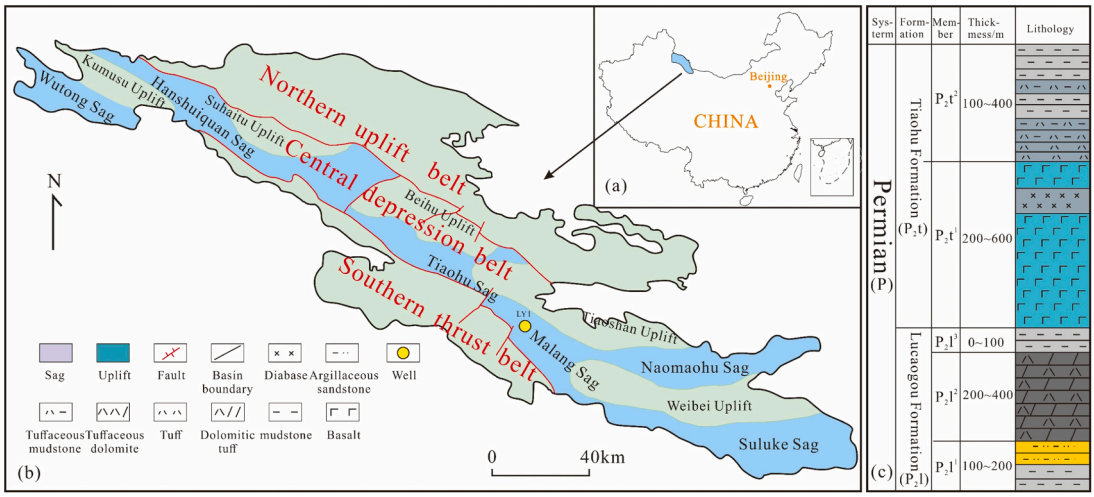

Fig. 1. (a) Geographical location of the Santanghu Basin; (b) Geologic map of the Santanghu Basin; (c) Stratigraphic column of the P_2l_2.

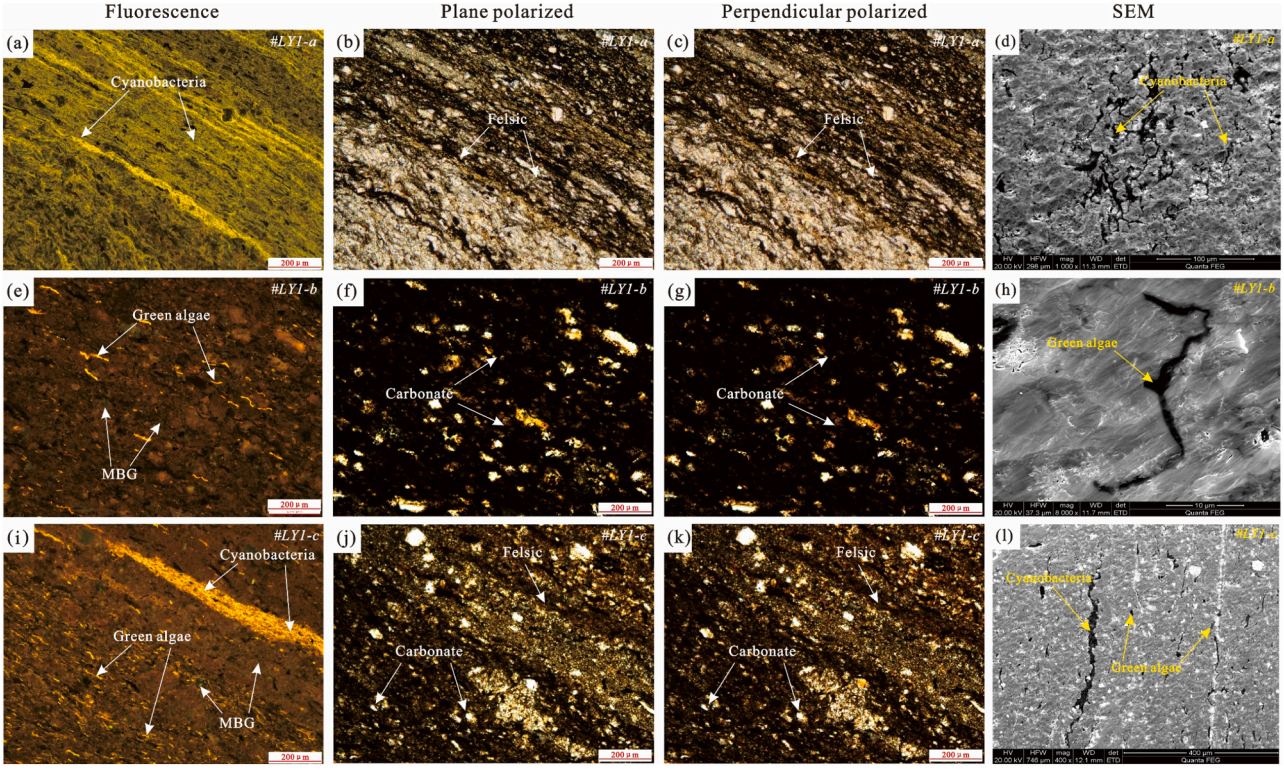

Fig. 2. Microscopic and SEM images of the investigating samples. (a-c) Cyanobacteria exhibiting yellow fluorescence are associated with felsic minerals., Well LY1, 3303.5 m; (d) SEM image of cyanobacteria, Well LY1 3303.5 m; (e-g) Green algae exhibit orange fluorescence and remain abundant even in high-carbonate environments, with Mbg showing yellow-orange fluorescence, Well LY1 3342.4 m; (h) SEM image of green algae, Well LY1 3342.4 m; (i-k) Cyanobacteria with yellow-orange fluorescence are associated with felsic minerals, green algae with orange fluorescence are linked to carbonate minerals, and Mbg exhibits yellow-orange fluorescence, Well LY1 3294.1 m; (l) SEM image of cyanobacteria and green algae, Well LY1 3294.1 m. Abbreviations: Mbg, mineral bituminous groundmass.

heavier, and in the mixed sample is intermediate.

Hydrocarbon generation kinetics analysis was conducted on these three typical samples under both open and closed systems. In the closed system, hydrous pyrolysis was performed using an autoclave device. The resulting liquid hydrocarbons were subjected to quantitative and component analyses, while the gaseous hydrocarbons were quantitatively analyzed for their gas components, and the post-reaction rock samples were measured for Ro. It is noteworthy that each sample used in the hydrocarbon generation kinetic analyses was thoroughly mixed to avoid the effects of lacustrine fine-grained rock heterogeneity on the experimental results. Thus, the hydrocarbon generation kinetic analysis process can be considered a series of continuous test experiments. All experiments were conducted on freshly cut sample surfaces. Additionally, we collected data on crude oil density, viscosity, wax content, and group component analyses from 29 shale oil samples provided by the PetroChina Tuha Oilfield Company.

3.1. Kinetic analysis in an open system

Kinetic experiments on the three typical samples were conducted

using a Rock-Eval VI device, following procedures similar to those described by Yu et al. [16] and Li et al. [11]. First, four 100 mg powdered parallel samples were prepared from each sample, and the instrument was set to activation energy analysis mode. One sample was placed in the crucible and heated at a constant temperature of 200°C for 5 minutes. Then, the sample was heated from 200°C to 600°C at different heating rates. The procedure was repeated with different heating rates after each reaction, and the heating rates used in this study were 10 °C/min, 30 °C/min, 40 °C/min, and 50 °C/min. Finally, data on cumulative hydrocarbon generation and activation energy at different heating rates were collected, and temperature-hydrocarbon generation rate curves were plotted.

3.2. Hydrous pyrolysis

Hydrous pyrolysis experiments on the three samples were conducted using a GPM-3 autoclave device with an approximate continuous testing approach. First, the samples were crushed into small pieces approximately 1×1×1 cm, thoroughly mixed, and divided into seven portions, each weighing more than 15 g. For each heating cycle, 15 g of the sample were placed into a high-pressure reactor along with about 15 ml of deionized water. The reactor chamber was then evacuated and observed for 5 minutes to ensure good airtightness, after which the samples were heated to the set temperatures at a rate of 2 °C/min and held at each temperature for 48 hours. The set temperatures for this experiment were 280°C, 300°C, 320°C, 340°C, 350°C, 370°C, and 400°C. After the experiment, gaseous hydrocarbons were collected using the water displacement method with a supersaturated NaCl solution. The collected liquid hydrocarbons included three phases: expelled oil, absorbed oil, and residual oil. Expelled oil was washed out directly from the reactor with dichloromethane, absorbed oil was obtained by soaking the post-reaction sample for 30 minutes, and residual oil was extracted from the post-reaction rock using Soxhlet extraction. These liquid hydrocarbons were separated into saturated hydrocarbons, aromatic hydrocarbons, resins, and asphaltenes using chromatography columns packed with alumina and silica gel, allowing for the determination of their relative contents at different maturities. Additionally, an Agilent 6890 four-valve, five-column multidimensional gas chromatograph was

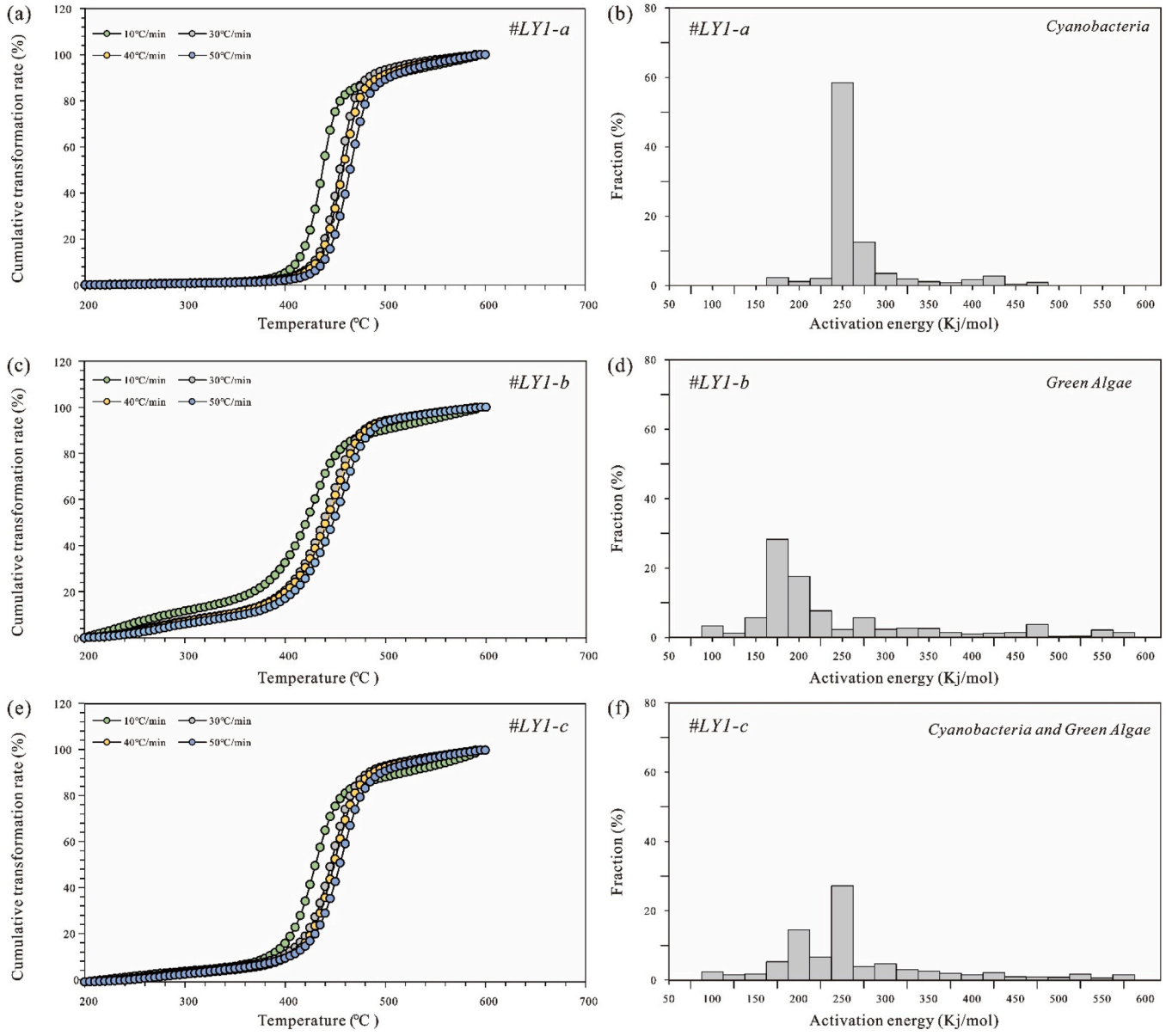

Fig. 3. Cumulative transformation rate (%) with different temperature during pyrolysis of the samples LY1-a (a), LY1-b (c), and LY1-c (e) of the investigating samples; Activation energy distribution and frequency factor of samples LY1-a (b), LY1-b (d), and LY1-c (f) of the samples in this study.

used to analyze the collected gases, differentiating between hydrocarbon and non-hydrocarbon gases. The detailed procedures for TOC, Rock-Eval, organic petrology, SEM, Ro analysis, and carbon isotope analysis are provided in the Supplementary Material.

4. Results and discussion

4.1. Differences in hydrocarbon generation rates based on activation energy

The Hydrocarbon Transformation Rate (HTR) curves of the three samples exhibit different characteristics (Fig. 3a, c, and e; Table S2). Generally, an HTR of 10 % and 90 % corresponds to the lower limit of effective hydrocarbon source rock generation and the hydrocarbon equilibrium point, respectively [47]. An HTR of 10 %-25 %, 25 %-65 %, and 65 %-90 % represents the early, main, and late stages of hydrocarbon generation, respectively [48]. Under different heating rates, the temperatures at which the three samples begin hydrocarbon generation (HTR = 10 %) vary, with sample LY1-a ranging from 415°C to 440°C (avg. 430°C), sample LY1-b from 285°C to 360°C (avg. 333.75°C), and sample LY1-c from 380°C to 400°C (avg. 393.75°C) (Table S3). Generally, the higher the heating rate, the higher the temperature at which hydrocarbon generation begins, which may be related to kinetic effects and heat transfer processes, as many researchers have concluded similar results [49,50]. This characteristic is most evident in sample LY1-b, where the temperature difference between heating at 10 °C/min and 50 °C/min is 75°C, and regardless of the heating rate, sample LY1-b begins hydrocarbon generation the earliest, followed by sample LY1-c and sample LY1-a, with LY1-b requiring an average temperature nearly 100°C lower than sample LY1-a to start generating hydrocarbons (Table S3). During the main hydrocarbon generation stage (HTR = 25 %-65 %), the hydrocarbon generation characteristics of the three samples also differ significantly. Firstly, before reaching the main hydrocarbon generation stage, sample LY1-a requires a higher reaction temperature, averaging about 445°C, while sample LY1-b requires only around 407°C, and sample LY1-c falls in between at about 430°C (Table S3). Moreover, under different heating rates, the average temperature spans for the main hydrocarbon generation stage of samples LY1-a, LY1-b, and LY1-c are 17.5°C, 42.5°C, and 25°C, respectively. Therefore, during the main hydrocarbon generation stage, sample LY1-a exhibits concentrated oil generation with a higher HTR, whereas sample LY1-b and sample LY1-c have wider hydrocarbon windows and lower HTR. In the effective hydrocarbon generation stage (HTR = 10 %-90 %), the three samples display similar characteristics, with average temperature spans of 66.25°C, 155°C, and 105°C for samples LY1-a, LY1-b, and LY1-c, respectively (Table S3). However, during the late hydrocarbon generation stage (HTR = 65 %-90 %), the temperature spans of the three samples differ by less than 10°C (Table S3), showing no significant difference. The activation energy distribution characteristics of the three samples further validate the above analysis results. The activation energy distribution range and pre-exponential factor for samples LY1-a, LY1-b, and LY1-c are 175–500 kJ/mol and 2.88×10^{14} s^{-1}, 100–625 kJ/mol and 9.87×10^{14} s^{-1}, and 100–600 kJ/mol and 2.58×10^{14} s^{-1}, respectively (Fig. 3b, d, and f; Table S4). In the activation energy range of 250–275 kJ/mol, the HTR for sample LY1-a can reach 58.47 %, while the activation energy distribution for hydrocarbon generation in sample LY1-b and sample LY1-c is more dispersed, indicating that oil generation in sample LY1-a is more concentrated.

The hydrocarbon generation characteristics reflect the differences in hydrocarbon generation among samples predominantly composed of cyanobacteria, green algae, and their mixtures. When the OM is mainly cyanobacteria origin (sample LY1-a), the activation energy required to start hydrocarbon generation is higher, and the hydrocarbon generation process is more concentrated. In contrast, when the OM is mainly green algae origin (sample LY1-b), the activation energy required is lower, and the process is more dispersed. For mixed OM (sample LY1-c), the hydrocarbon generation is also dispersed but still shows characteristics of cyanobacteria hydrocarbon conversion. For instance, LY1-c has an HTR of 27.17 % in the activation energy range of 250–275 kJ/mol (Fig. 3; Table S4), reflecting the influence of cyanobacteria-derived OM on its hydrocarbon generation characteristics. Such activation energy distribution characteristics are not surprising. Previous studies have shown that algal OM in saline lacustrine environments often requires higher activation energy during decomposition. For instance, the activation energy peak for OM in the saline lacustrine Qingshuihe Formation of the Cretaceous in the Junggar Basin is approximately 300 kJ/mol, while the peak for the OM in the saline lacustrine Paleogene Anjihaihe Formation is around 340 kJ/mol [16]. Additionally, the activation energy distribution for OM in the Permian Lucaogou Formation in the Jimusaer Sag of the Junggar Basin ranges from 100 to 600 kJ/mol, with a peak around 310 kJ/mol [51]. In contrast, the activation energy for OM in the freshwater or brackish water Chang 7 Member of the Ordos Basin is significantly lower [52,53]. The differences in hydrocarbon generation between OM mainly from green algae and that mainly from cyanobacteria may be related to their cell structures and biochemical compositions [54,55]. Green algae, being eukaryotes with more complex cell structures including nuclei, chloroplasts, and mitochondria [56], allow multiple metabolic activities to occur simultaneously, which affects the interactions between molecules and reduces bond energy. On the other hand, cyanobacteria have unique metabolic pathways, such as oxygenic photosynthesis, which produce more complex organic compounds that require higher energy to break down during pyrolysis [57–59]. In terms of cell chemical composition, higher salinity may lead to thinner or even absent cell walls in green algae to balance osmotic pressure [60], and green algae contains a higher proportion of lipids (e.g., oils and fatty acids), which have simpler molecular structures. These lipids break and recombine more easily into hydrocarbons when heated, resulting in lower activation energy required for hydrocarbon generation [61]. In contrast, cyanobacteria have higher proportions of proteins, carbohydrates, and complex polysaccharides (e.g., peptidoglycan) [62–64], which require more energy to decompose due to their complex molecular structures. Consequently, shale with green algae as the main OM has a broader oil generation window, while shale with cyanobacteria as the main OM exhibits late but concentrated oil generation.

4.2. Differences in hydrocarbon generation characteristics based on hydrous pyrolysis

4.2.1. Hydrocarbon yield characteristics

Three samples were subjected to hydrous pyrolysis in autoclave device, yielding both liquid and gaseous hydrocarbons (Table S5). All three samples primarily produced oil, with the amount of generated oil initially increasing and then decreasing (Fig. 4a). In the Ro < 1.0 % range, the amount of generated gaseous hydrocarbons was very low (<70 mg/g TOC) (Fig. 4b). Significant amounts of gaseous hydrocarbons were only produced during the higher maturity stage of oil cracking (Ro > 1.0 %), which is consistent with the hydrocarbon generation characteristics of bacteria and algae [14]. Regarding the liquid hydrocarbon yield, using 100 mg/g TOC as the threshold for substantial oil production, the sample rich in green algae (sample LY1-b) began producing substantial oil at an earlier stage (Ro approximately 0.78 %), the sample rich in cyanobacteria (sample LY1-a) entered the substantial oil production stage later (Ro approximately 0.88 %), and the sample with mixed algae (sample LY1-c) began substantial oil production at an intermediate stage (Ro approximately 0.82 %) (Table S5). Additionally, the oil generation peaks of the three samples differed, with the peak for sample LY1-a occurring at Ro = 1.06 % and a maximum oil yield of about 581.11 mg/g TOC, sample LY1-b's peak at Ro = 0.95 % with a maximum oil yield of around 360.65 mg/g TOC, and sample LY1-c's peak at Ro = 1.01 % with a maximum oil yield of roughly 425.4 mg/g TOC (Table S5).

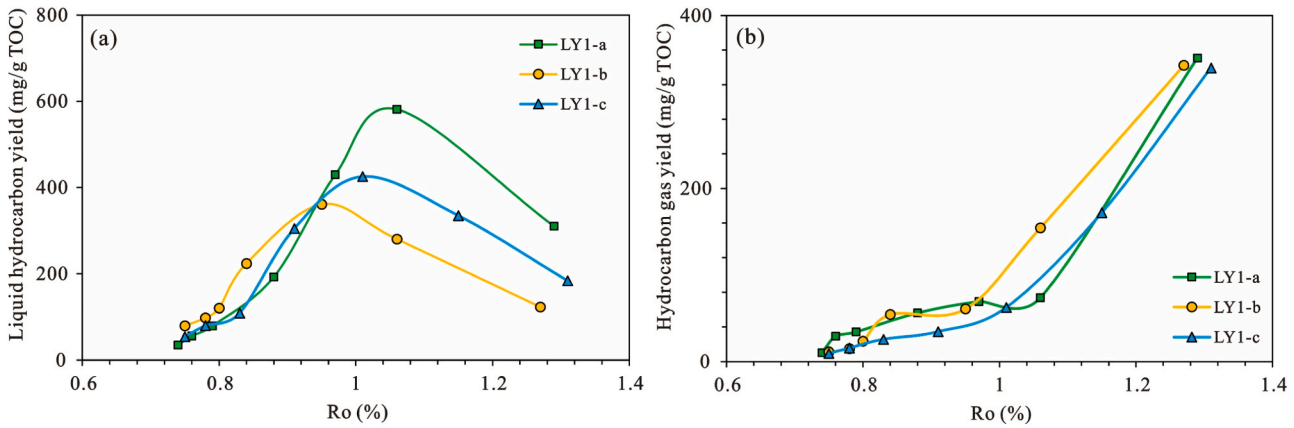

Fig. 4. The relationship between liquid hydrocarbon yield (a) and hydrocarbon gas yield (b) with Ro of the investigating samples during the hydrous pyrolysis experiment.

The hydrocarbon generation characteristics from hydrous pyrolysis of the three samples align with the activation energy analysis results. Based on this, hydrocarbon generation models for different types of the OM in the P_2l_2 shale were established: the "green algae origin - early hydrocarbon generation - early oil peak - broad oil window model" (GEEB model) (Fig. 5a) and the "cyanobacteria origin - late hydrocarbon generation - late oil peak - concentrated oil generation model" (CLLC model) (Fig. 5b). Additionally, considering the principle of mass conservation, where approximately 50–60 % of crude oil is converted into hydrocarbon gas during cracking [65–67], the GEEB model can generate 290.56–348.67 mg/g TOC of hydrocarbon gas, while the CLLC model can produce 180.33–216.39 mg/g TOC. Moreover, kerogen cracking can yield around 100 mg/g TOC of hydrocarbon gas [68]. Therefore, the GEEB model can produce approximately 390.56–448.67 mg/g TOC of hydrocarbon gas, while the CLLC model can generate about 280.32–316.39 mg/g TOC. Given that the current maturity of OM in the P_2l_2 is generally between 0.5 % and 1.2 %, and no tight gas reservoirs have been found [35,39], it is likely that some of the early-generated hydrocarbon gases are present as condensate gas, considering the differences between simulation conditions and actual geological conditions.

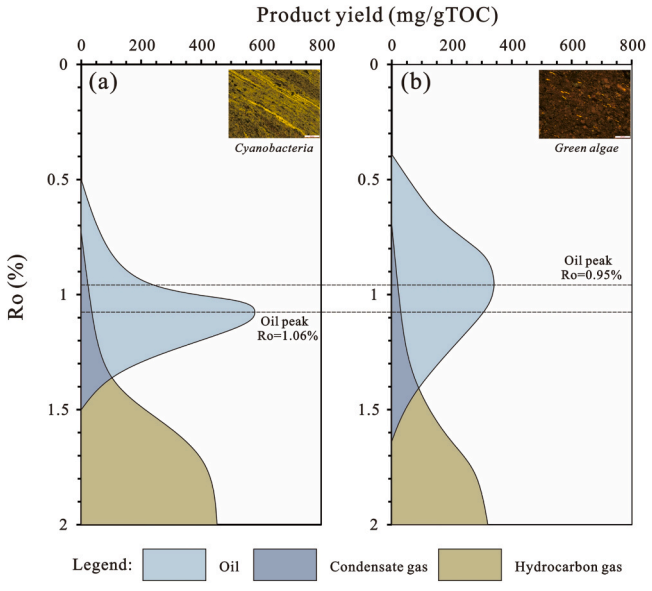

Fig. 5. The hydrocarbon generation model of cyanobacteria-rich shale (a) and green algae-rich shale (b) in the investigating samples.

4.2.2. Components of liquid hydrocarbons

The components of crude oil refer to the proportions of saturated hydrocarbons, aromatic hydrocarbons, resins, and asphaltenes present in the oil [69]. Crude oil with a higher concentration of small molecular compounds, such as saturated and aromatic hydrocarbons, generally has lower density and viscosity, signifying superior quality, whereas oil with a greater content of resins and asphaltenes tends to exhibit higher density and viscosity, indicating inferior quality [25,27,70]. Additionally, it is generally believed that as the maturity of crude oil increases, the proportion of large molecular compounds like resins and asphaltenes decreases, leading to an improvement in oil quality [71]. However, some researchers argue that crude oil density initially increases and then decreases with rising maturity, reaching its maximum near the oil generation peak [28,72]. In this study, a significant negative correlation was found between the content of saturated hydrocarbons and the density and viscosity of crude oil (Fig. 6a and b; Table S6). Conversely, the density and viscosity of crude oil increased with the rising content of aromatic hydrocarbons, resins, and asphaltenes. This finding contrasts with previous research suggesting that an increase in aromatic hydrocarbons, being small molecular compounds, improves oil quality [25]. This discrepancy may be related to the molecular structure of aromatic hydrocarbons, which typically feature benzene rings and polycyclic aromatic structures, making the molecules more compact [73]. Additionally, the strong bonding energy of the carbon-carbon bonds in aromatic hydrocarbons contributes to forming a stable and dense structure [74]. The sum of aromatic hydrocarbons, resins, and asphaltenes (heavy component content) showed a significant correlation with crude oil density and viscosity (Fig. 6c; Table S6), indicating that their relative content is a key factor affecting oil quality. There was also a strong positive correlation between wax content and the proportion of saturated hydrocarbons in crude oil (Fig. 6d; Table S6), but no obvious correlation with the relative content of aromatic hydrocarbons, resins, and asphaltenes. This is not surprising given that, as the OM in the P_2l_2, although composed of bacteria and algae [29,31,32,42], has a molecular composition with a very high proportion of medium and high molecular weight *n*-alkanes, predominantly *n*-C_{23} and *n*-C_{25} [32,75,76], which are more prone to crystallize and form wax at lower temperatures [77].

Further research revealed that during hydrous pyrolysis of the three samples, the heavy component content in the three liquid hydrocarbon phases initially increased and then decreased with increasing maturity (Fig. 7a, b, and c; Table S7). Additionally, the relative heavy component content followed the pattern of expelled oil > absorbed oil > residual oil (Fig. 7a, b, and c), a phenomenon similar to the differentiation effect of crude oil components under geological conditions, where smaller molecular weight *n*-alkanes and free-state heavy components are easily expelled from tight rocks, while adsorbed heavy components and cycloalkanes tend to remain in rock pores due to capillary forces [78,

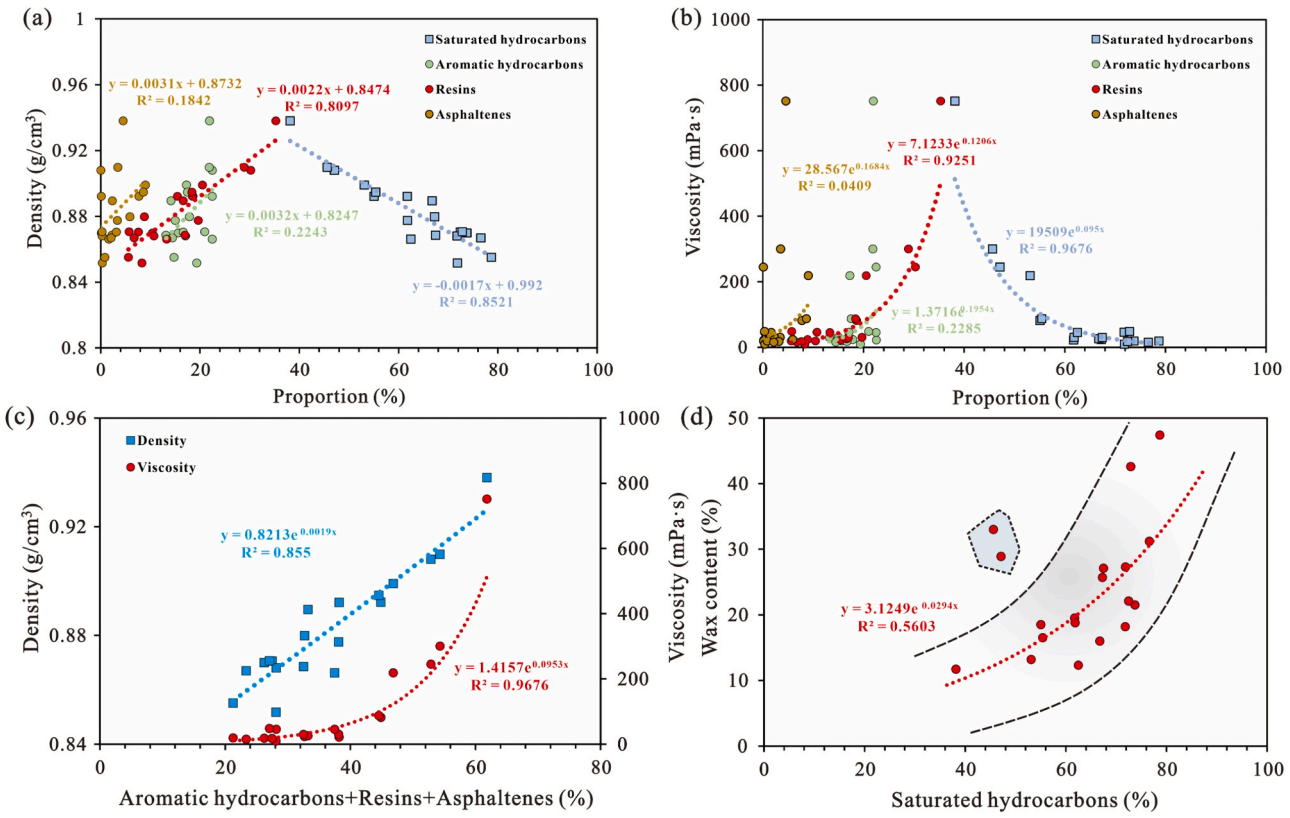

Fig. 6. The relationship between the physical properties of crude oil and the components of crude oil. Correlation between the relative contents of saturated hydrocarbons, aromatic hydrocarbons, resins, and asphaltenes with crude oil density (a) and Viscosity (b); (c) Correlation between heavy component content (aromatic hydrocarbons, resins, and asphaltenes) and crude oil density and viscosity; (d) Correlation between the relative content of saturated hydrocarbons and wax content in crude oil.

79]. The color changes of crude oil in dichloromethane at different maturities also support this conclusion, as the maturity increases, the color of liquid hydrocarbons changes from colorless to brown (black) and then gradually to light yellow (Fig. 7d-l), reflecting changes in the heavy component content of the liquid hydrocarbons [11,16], which can also be explained by the theory that oil quality is poorest at the oil generation peak [45]. Sample LY1-a reaches its oil generation peak later, and thus at 350°C and 370°C, the hydrocarbon color is the darkest (Fig. 7d, g, and j), corresponding to the highest heavy component content, with the heavy component content in the residual oil reaching 65.61 % at Ro = 1.06 %, nearly tripling from the initial evolution stage. Sample LY1-b, with a lower activation energy for oil generation and a lower Ro value at the oil generation peak, shows the darkest hydrocarbon color around 350°C (Ro = 0.8 %) (Fig. 7e, h, and k), with a heavy component content in the residual oil of about 54.39 %. Overall, the heavy component content in the liquid hydrocarbons of sample LY1-b changes less significantly compared to the initial evolution stage, supporting the conclusion of its wider oil window. The hydrocarbon generation characteristics of sample LY1-c are similar to those of the other two samples, exhibiting both an early oil generation peak (darkest color at 350°C) and a high heavy component content in the generated hydrocarbons (Fig. 7f, i, and l). Notably, after Ro > 0.95 %, the heavy component content in all three liquid hydrocarbon phases of sample LY1-b decreases rapidly (Fig. 7a, b, and c), contrasting sharply with sample LY1-a, where the heavy component content remains high and decreases slowly during the maturity stage. Thus, based on the hydrocarbon generation models proposed in Section 4.1, OM mainly of green algae origins (sample LY1-b) also exhibit the characteristic of generally lower heavy component content in the generated liquid hydrocarbons, while OM predominantly of cyanobacteria origins (sample LY1-a) show significant variations in heavy component content during evolution.

4.3. Geological implication

The research area has Ro values ranging from 0.51 % to 1.10 % (average 0.74 %), showing a good correlation between Ro and depth (Fig. 8). Using this linear relationship, the approximate burial depths corresponding to different thermal evolution stages for the three samples were calculated (Table S8). The results indicate that the simulated burial depths for samples LY1-a, LY1-b, and LY1-c are 2981.5m-4214.2 m, 3011.3m-4248.3 m, and 3011.3m-4179.6 m, respectively (Table S8), a depth range that well covers the main exploration depths of the current P_2l_2 shale oil [34,35,80,81]. Based on the relationship between heavy component content and crude oil density and viscosity shown in Fig. 6c, the density and viscosity of different phases of crude oil generated at various thermal evolution stages for the three samples were calculated (Table S8). The calculations show that the density and viscosity of liquid hydrocarbons generated by sample LY1-a range from 0.85 g/cm^3 to 0.93 g/cm^3 (average 0.89 g/cm^3) and 10.03 mPa·s to 735.55 mPa·s (average 151.01 mPa·s), respectively (Table S8). For sample LY1-b, the density and viscosity range from 0.85 g/cm^3 to 0.91 g/cm^3 (average 0.88 g/cm^3) and 10.63 mPa·s to 252.42 mPa·s (average 79.01 mPa·s), respectively. For sample LY1-c, the density and viscosity range from 0.86 g/cm^3 to 0.92 g/cm^3 (average 0.89 g/cm^3) and 11.13 mPa·s to 380.6 mPa·s (average 102.08 mPa·s), respectively. Additionally, collected crude oil samples from depths of 2744.5 m to 3947 m (Table S6) have densities ranging from 0.85 g/cm^3 to 0.94 g/cm^3 (average 0.89 g/cm^3) and viscosities from 9.07 mPa·s to 1106 mPa·s (average 130.86 mPa·s), which are consistent with the density and viscosity distributions obtained from the hydrous pyrolysis of the three samples. Therefore, the simulation results can be used to explain the distribution characteristics of crude oil density and viscosity.

As burial depth increases, the density and viscosity of crude oil and

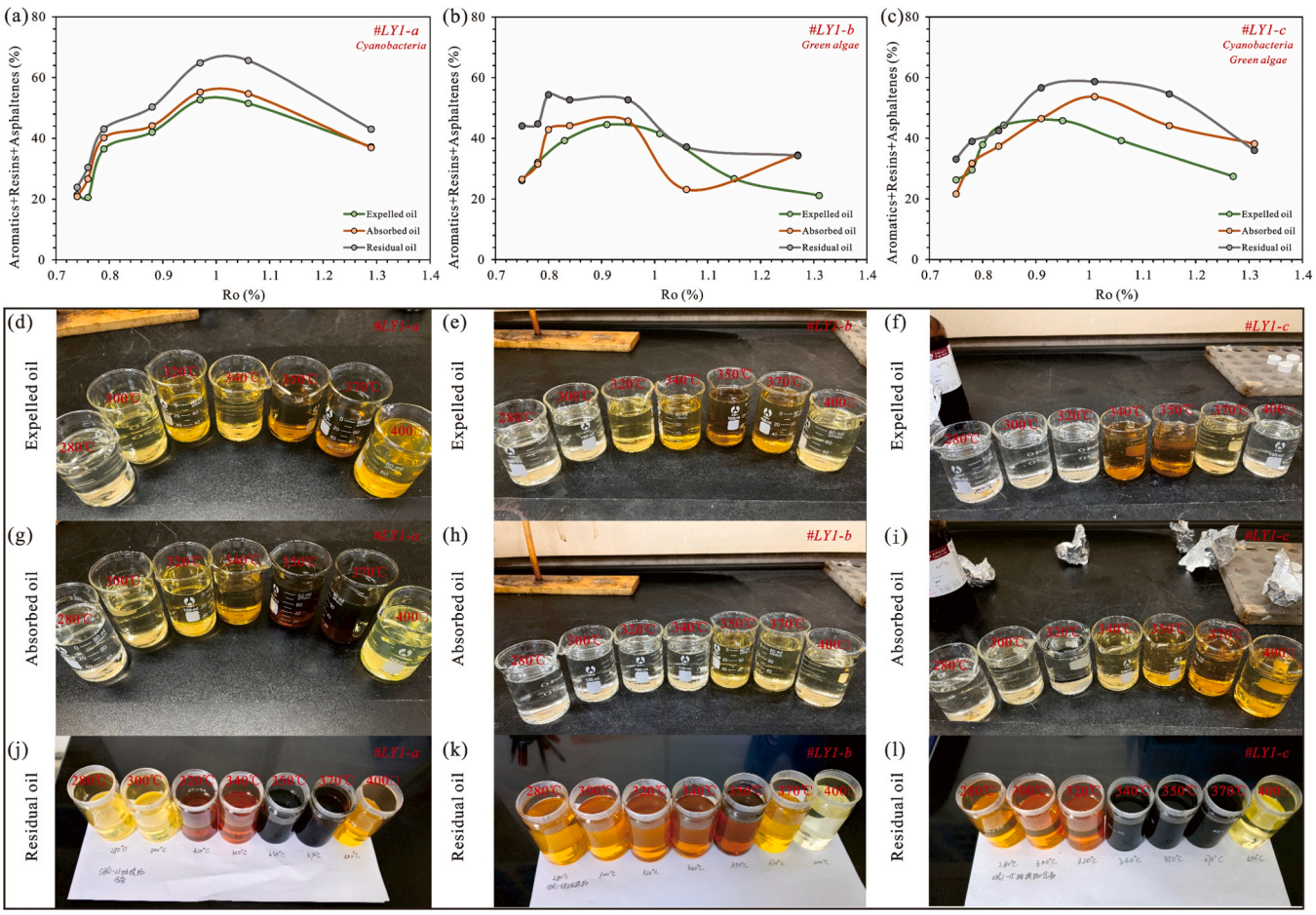

Fig. 7. Changes in liquid hydrocarbon component during hydrous pyrolysis experiment. Relationship between the component of three phases of liquid hydrocarbons and Ro for samples LY1-a (a), LY1-b (b), and LY1-c (c) during hydrous pyrolysis experiment; Component changes of expelled oil (d, e, and f), absorbed oil (g, h, and i), and residual oil (j, k, and l) for samples LY1-a, LY1-b, and LY1-c during hydrous pyrolysis experiment.

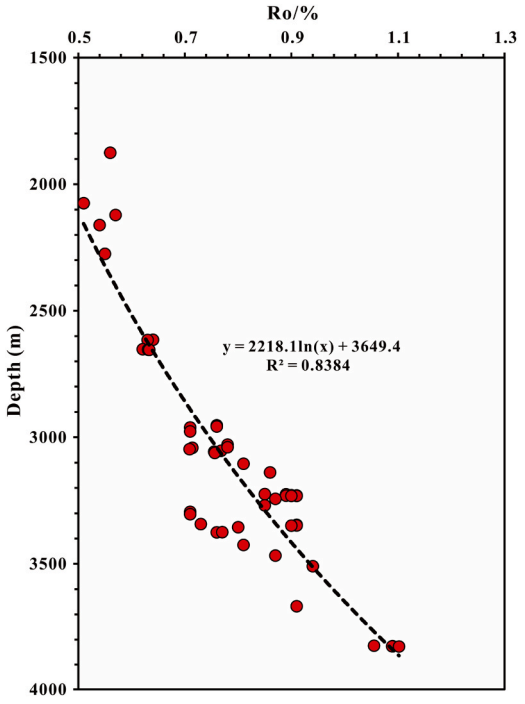

Fig. 8. Relationship between Ro and depth of the P_2l_2.

hydrous pyrolysis liquid hydrocarbons initially rise and then fall with increasing maturity (Fig. 9), reflecting the influence of OM differences on the density and viscosity of crude oil. However, even at the same depth, crude oil samples can exhibit variations in density and viscosity due to the differential enrichment of OM [16,28]. Additionally, the component differentiation effect caused by primary migration within the source rock can also influence these variations [79]. During primary migration, lighter components, due to their lower molecular weight, more easily migrate through microfractures and pores, resulting in a relative increase in the proportion of heavy components remaining in the source rock, thereby increasing the density and viscosity of the crude oil [82,83]. Therefore, under the same degree of OM enrichment, the density and viscosity of residual heavy hydrocarbons are more consistent with the physical evolution curve of residual oil in the experiment, while the density and viscosity of more mobile free-state crude oil are more consistent with those of expelled oil and absorbed oil.

The Lucaogou Formation develops upper, middle, and lower sweet spots, while the P_2l_2 mainly develops upper and middle sweet spots [1, 80,84]. the P_2l_2 is generally a source-reservoir integrated shale oil reservoir, where hydrocarbons generated by the source rock primarily undergo primary migration and in-source enrichment [35,36,38,42]. The main lithologies of the P_2l_2, which can be classified based on the relative content of felsic and carbonate minerals into tuff, dolomitic tuff, tuffaceous dolomite, and dolomite [31,84], are well correlated with volcanic eruption cycles: tuff and dolomitic tuff are primarily deposited during periods of intense volcanic activity, while dolomite and tuffaceous dolomite are deposited during weaker volcanic activity or

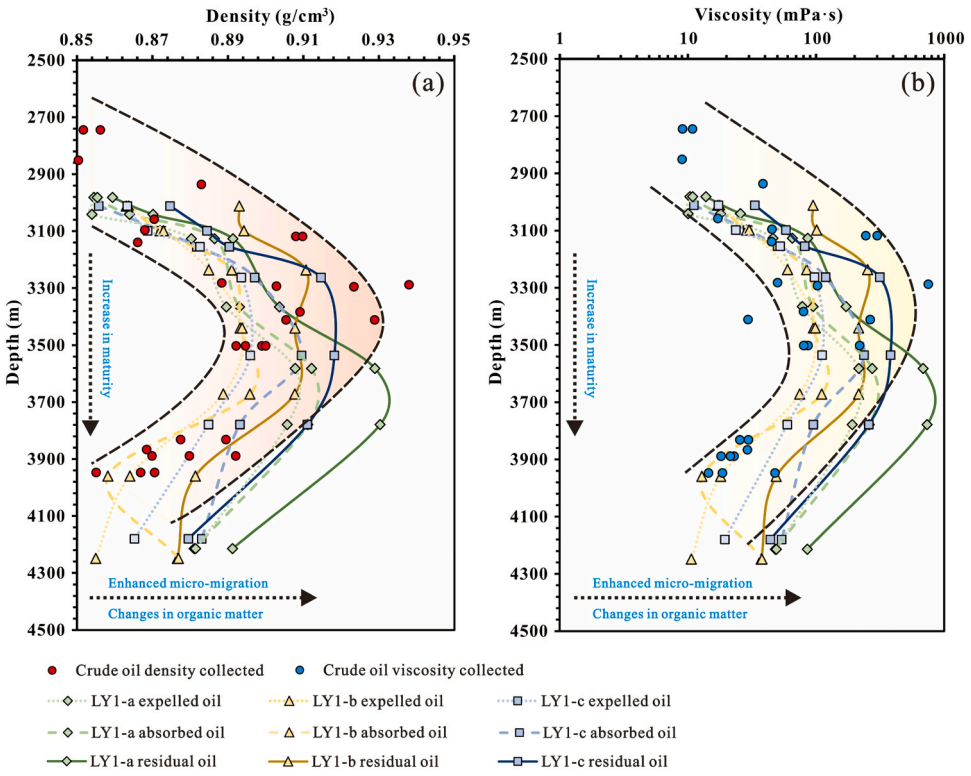

Fig. 9. Relationship between depth and the properties of crude oil and hydrous pyrolysis liquid hydrocarbons.

volcanic hiatuses [32]. The OM in the P_2l_2 dolomite is mainly green algae, while in tuffaceous dolomite and dolomitic tuff, it consists of green algae or a mixture of green algae and cyanobacteria, with cyanobacteria being the dominant OM in some dolomitic tuff and tuff. Due to the short duration of intense volcanic eruptions, the organic composition of the P_2l_2 is dominated by green algae or a mix of green algae and cyanobacteria. Consequently, the evolution of crude oil density and viscosity are found to be more similar to those of samples LY1-b and LY1-c (Fig. 9). If the crude oil samples are assumed to be derived from dolomitic tuff or tuff formed during volcanic eruptions, their density and viscosity evolution trends might resemble those of sample LY1-a.

The dolomitic reservoirs in the P_2l_2 formation are characterized by good physical properties and pore structures, having undergone multiple diagenetic alterations, making them favorable reservoirs [45,80]. Additionally, these reservoirs predominantly contain green algae-derived OM, which generates significant amounts of liquid hydrocarbons at relatively low maturity levels, and throughout the evolution process, the produced liquid hydrocarbons exhibit relatively low density and viscosity, making these reservoirs advantageous targets for the P_2l_2 shale oil exploration. However, it is noteworthy that for sample LY1-a, the density and viscosity of the generated liquid hydrocarbons only increase significantly at burial depths greater than 3500 m (Ro > 0.95 %). Therefore, when Ro < 0.95 %, dolomitic tuff or tuff reservoirs formed during periods of intense volcanic eruptions, if of good quality, can also be favorable targets for the P_2l_2 shale oil exploration. Conversely, when Ro > 0.95 %, even if the tuff reservoirs have undergone favorable diagenetic alterations, the hydrocarbons present will have very high density and viscosity, making them less favorable for shale oil exploration.

5. Conclusions

The P_2l_2 shale primarily contains two types of OM: cyanobacteria and green algae. Analysis of hydrocarbon generation activation energy and hydrous pyrolysis experiments reveals differences in their hydrocarbon generation characteristics. OM mainly derived from green algae requires lower activation energy to initiate significant hydrocarbon production, exhibits a broader oil window, and lacks a pronounced oil generation peak. In contrast, OM mainly derived from cyanobacteria generates limited hydrocarbons at low maturity stages but shows a concentrated oil generation peak. Based on these observations, two hydrocarbon generation models were established: the GEEB model and the CLLC model.

Aromatic hydrocarbons, resins, and asphaltenes show a positive correlation with crude oil density and viscosity, constituting the heavy components that degrade oil quality. Hydrous pyrolysis of samples containing green algae, cyanobacteria, and a mixture of both shows that the heavy component content in their liquid hydrocarbons initially increases and then decreases with increasing maturity. Additionally, at different evolutionary stages, the heavy component content follows the pattern of residual oil > absorbed oil > expelled oil. Compared to cyanobacteria, green algae exhibit relatively smaller changes in heavy component content during evolution. Furthermore, the color changes of crude oil in dichloromethane effectively reflect the variations in heavy component content.

The density and viscosity of the three types of liquid hydrocarbons from the hydrous pyrolysis experiment were calculated, along with their corresponding relationship to depth, and then compared to the physical property distribution of the P_2l_2 crude oil. The results indicate that differences in OM hydrocarbon generation characteristics control the density and viscosity of the P_2l_2 crude oil. Furthermore, crude oil samples from the same depth exhibit significant variations in density and viscosity, which may be influenced not only by the evolution of OM but also by the differentiation effect of in-source oil migration. This underscores the rationale for distinguishing phases in liquid hydrocarbons during hydrous pyrolysis experiments, making this analytical method practically significant for predicting favorable targets in shale oil exploration.

CRediT authorship contribution statement

Jilun Kang: Supervision, Resources, Project administration. **Xiongfei Xu:** Supervision, Investigation. **Wei Zhang:** Supervision, Project administration. **Hui Liang:** Validation, Supervision, Resources, Project administration. **Miao Liu:** Visualization, Supervision, Investigation, Data curation. **Gang Gao:** Writing – review & editing, Supervision, Funding acquisition, Data curation. **Miao Yu:** Writing – original draft, Visualization, Data curation, Conceptualization.

Declaration of Competing Interest

We declare that we have no financial and personal relationships with other people or organizations that can inappropriately influence our work, there is no professional or other personal interest of any nature or kind in any product, service and/or company that could be construed as influencing the position presented in, or the review of, the manuscript entitled "***Differential hydrocarbon generation characteristics of organic matter with green algae and cyanobateria origins in the Permain Lucaogou Formation of the Santanghu Basin***".

Acknowledgments

Thanks to PetroChina Tuha Oilfield Company for the funding. (No. YJYHZC2022). Thanks for the guidance of experts from Exploration and Development Research Institute of Tuha Oilfield Company of PetroChina. We sincerely thank the Editor-in-Chief and the anonymous reviewers for their insightful comments, which have significantly enhanced the quality of this paper.

Declaration of competing interest

The authors declare no known competing financial interests or personal relationships that could have influenced the work reported in this paper.

Appendix A. Supporting information

Supplementary data associated with this article can be found in the online version at doi:10.1016/j.jaap.2024.106821.

Data Availability

Data will be made available on request.

References

[1] B. Liu, J.X. Shi, X.F. Fu, Y.F. Lv, X.D. Sun, L. Gong, Y.F. Bai, Petrological characteristics and shale oil enrichment of lacustrine fine-grained sedimentary system: a case study of organic-rich shale in first member of Cretaceous Qingshankou Formation in Gulong Sag, Songliao Basin, NE China, Pet. Explor. Dev. 45 (05) (2018) 828–838, https://doi.org/10.1016/j.petrol.2018.09.013.

[2] Z. Yang, C.N. Zou, L.H. Hou, S.T. Wu, S.H. Lin, X. Luo, L.J. Zhang, Z.Y. Zhao, J. W. Cui, S.Q. Pan, Division of fine-grained rocks and selection of "sweet sections" in the oldest continental shale in China: taking the coexisting combination of tight and shale oil in the Permian Junggar Basin, Mar. Pet. Geol. 109 (2019) 339–348, https://doi.org/10.1016/j.marpetgeo.2019.04.017.

[3] F. Wang, R. Chen, W. Yu, J.C. Tian, X.W. Liang, X.F. Tan, L. Gong, Characteristics of lacustrine deepwater fine-grained lithofacies and source-reservoir combination of tight oil in the Triassic Chang 7 member in Ordos Basin, China, J. Pet. Sci. Eng. (2021) 108429, https://doi.org/10.1016/j.petrol.2021.108429.

[4] J.H. Li, X.L. Shan, X. Song, W.T. He, Evaluation of the organic matter product of Huadian oil shale during pyrolysis using multiple approaches: guidance for the in situ conversion of oil shale, J. Anal. Appl. Pyrolysis 167 (2022), https://doi.org/10.1016/j.jaap.2022.105587.

[5] L.H. Hou, K. He, J. Zhai, J.K. Mi, N. Weng, Compositional kinetics for hydrocarbon evolution in the pyrolysis of the Chang 7 organic matter: implications for in-situ conversion of oil shale, J. Anal. Appl. Pyrolysis 167 (2022) 105434, https://doi.org/10.1016/j.jaap.2022.105434.

[6] W.X. Han, X. Luo, S.Z. Tao, S.H. Lin, J.Z. Liu, Y.T. Yang, Activation energy and organic matter structure characteristics of shale kerogen and their significance for the in-situ conversion process of shale oil, Fuel 370 (2024) 131823, https://doi.org/10.1016/j.fuel.2024.131823.

[7] X.D. Liu, Q. Wang, W.L. Jia, J.Z. Song, P.A. Peng, Pyrolysis of an organic-rich shale containing type II kerogen before and after oil generation and expulsion: implications for the generation of late hydrocarbon and hydrogen gases, J. Anal. Appl. Pyrolysis 173 (2023), https://doi.org/10.1016/j.jaap.2023.105605.

[8] B. Pang, X.Q. Pang, B. Luo, D.Y. Zheng, Z. Xu, S.Y. Zhang, J.Q. Chen, Influence of the Emeishan basalt eruption on hydrocarbon generation and expulsion characteristics of Sinian (Ediacaran) algal dolomite in Sichuan Basin, J. Anal. Appl. Pyrolysis 169 (2023), https://doi.org/10.1016/j.jaap.2023.105653.

[9] R.H. Zheng, Y.F. Wang, Z.P. Li, Z.H. Zhang, G.L. Wang, H. Zhang, Differences and origins of hydrocarbon generation characteristics between mudstone and shale in the Seventh Member of the Yanchang Formation, Ordos Basin, China, Int. J. Coal Geol. 257 (2022), https://doi.org/10.1016/j.coal.2022.104075.

[10] M. Guan, X.P. Liu, Z.J. Jin, J. Lai, B. Sun, P.P. Zhang, K.F. Chen, The evolution of pore structure heterogeneity during thermal maturation in lacustrine shale pyrolysis, J. Anal. Appl. Pyrolysis 169 (2022) 105501, https://doi.org/10.1016/j.jaap.2022.105501.

[11] G.X. Li, C.L. Liu, R.S. Awan, X.Y. Yang, D.H. Feng, F.L. Wang, X.X. Zeng, H. Yang, J. J. Su, Y.P. Wu, T.Z. Yang, Z.G. Ding, Z.X. Chen, The implication of kinetics characteristics of modern organisms for the hydrocarbon generation evolution of organic matter components in the lacustrine source rocks: a case study of the Dongying Formation from the Bozhong Sag, Bohai Bay Basin, J. Anal. Appl. Pyrolysis 177 (2024) 106328, https://doi.org/10.1016/j.jaap.2024.106328.

[12] Z.S. Luan, J.F. Du, P.C. Sun, L.Y. Hou, C. Ding, Progress in thermal simulation studies of hydrocarbon generation and its constraints on unconventional oil and gas accumulation, China Coal Geol. 33 (07) (2021) 19–26+71.

[13] M. Yu, G. Gao, J. Jin, W.Y. Ma, D. He, B.L. Xiang, K.T. Fan, M. Liu, Hydrocarbon generation simulation of coaly source rocks in the Lower combination on the southern margin of Junggar Basin and indications for oil and gas sources of well Gaotan 1, Pet. Geol. Exp. 44 (04) (2022) 687–697.

[14] X. Xie, J.K. Volkman, J. Qin, T. Borjigin, L. Bian, L. Zhen, Petrology and hydrocarbon potential of microalgal and macroalgal dominated oil shales from the Eocene Huadian Formation, NE China. Int. J. Coal Geol. 124 (2014) 36-47. https://doi.org/10.1016/j.coal.2013.11.010.

[15] Y.B. Quan, Z.Y. Chen, Y.M. Jiang, H. Diao, X.N. Xie, Y.C. Lu, X.B. Du, X.F. Liu, Hydrocarbon generation potential, geochemical characteristics and accumulation contribution of coal-bearing source rocks in the Xihu Sag, East China Sea Shelf Basin, Mar. Pet. Geol. 136 (2022), https://doi.org/10.1016/j.marpetgeo.2022.105701.

[16] M. Yu, G. Gao, W.Y. Ma, M. Liu, N. Zhou, Y.J. Zhang, D. He, K.T. Fan, L.L.B. Guo, J. Li, Hydrocarbon generation differences of shales composed of green algal and cyanobacteria: a case study of Mesozoic and Cenozoic saline lacustrine shales in Junggar Basin, NW China, Pet. Sci. 20 (06) (2023) 3348–3362, https://doi.org/10.1016/j.petsci.2023.05.005.

[17] W.E. Robinson, Kerogen of the Green River Formation, in: G. Eglinton, M.T. J. Murphy (Eds.), Organic Geochemistry, Springer, Berlin/Heidelberg/New York, 1969, pp. 619–637.

[18] A.C. Hutton, Petrographic approach to beneficiation of Australian oil shales, Fuel 66 (1987) 314–318, https://doi.org/10.1016/0016-2361(87)90103-1.

[19] W.D. Smith, C.J. St. Peter, R.D. Naylor, P.K. Mukhopadhyay, W.D. Kalkreuth, F. D. Ball, G. Macauley, Composition and depositional environment of major eastern Canadian oil shales, Int. J. Coal Geol. 19 (1991) 385–438, https://doi.org/10.1016/0166-5162(91)90053-Y.

[20] Q. Jiang, Q. Wang, Q. Cheng, C.M. Zhang, W.B. Liu, Preliminary analysis of the hydrocarbon generation kinetics characteristics of different component source rocks, . Pet. Geol. Exp. (05) (2005), 92-98+113.

[21] F. Wang, D.J. Zhang, G.J. Xu, Summation of hydrocarbon generation parameters for organic macerals and its application, Pet. Explor. Dev. 06 (2007) 696–701.

[22] J. Xu, C.M. Zhang, X.M. Xie, X.Q. Rui, Separation and geochemical characteristics of macerals in organic-rich source rocks, Pet. Geol. Exp. 40 (06) (2018) 828–835.

[23] Q.Q. Meng, J.Z. Qin, W.B. Liu, W.X. Hu, L.J. Zheng, Experimental study on hydrocarbon characteristics of multicellular macroscopic benthic algae, Acta Pet. Sin. 06 (2008) 822–826.

[24] M. Yu, G. Gao, X.Y. Zhao, M. Liu, W.Y. Ma, Y.J. Zhang, Sedimentary environment and a development model for source rocks rich in the green alga Pediastrum: a case study of the Paleogene Anjihaihe Formation in the Junggar Basin, northwest China, Int. J. Earth Sci. (Geol. Rundsch.) (2024), https://doi.org/10.1007/s00531-024-02415-9.

[25] S.J. Liu, G. Gao, J. Jin, D. Misch, X.S. Wu, G.Z. Gang, M. Wang, B.L. Xiang, W. Y. Ma, Mechanism of differential enrichment of shale oils in the upper and lower members of the Lucaogou Formation in the Jimusaer Sag, Junggar Basin, Mar. Pet. Geol. 142 (2022), https://doi.org/10.1016/j.marpetgeo.2022.105588.

[26] C.N. Zou, Z. Yang, G.S. Zhang, L.H. Hou, R.K. Zhu, S.Z. Tao, X.J. Yuan, D.Z. Dong, Y.M. Wang, Q.L. Guo, L. Wang, H.B. Bi, D.H. Li, N. Wu, Conventional and unconventional petroleum "orderly accumulation": Concept and practical significance, Pet. Explor. Dev. 41 (1) (2014) 14–30, https://doi.org/10.1016/S1876-3804(14)60002-7.

[27] J.W. Lin, X.M. Xie, Z.G. Wen, F.T. Wu, J. Xu, Z.L. Ma, L. Zhang, Geochemical comparison of oil expelled and retained during thermal simulation of Tasmania oil shale: group composition and isotope composition, Pet. Geol. Exp. 44 (01) (2022) 150–159.

[28] G. Gao, S.J. Liu, J. Jin, Z.H. Zhang, G.D. Liu, B.L. Xiang, Z.L. Huang, J.L. Kang, W. Z. Gang, New findings on the evolution law of crude oil physical properties and its implications for shale oil exploration, Acta Geol. Sin. 97 (05) (2023) 1561–1575.

[29] C.H. Paul, T. Fishman, G. Wu, G. Baugher, Organic petrology and geochemistry of mudrocks from the lacustrine Lucaogou Formation, Santanghu Basin, northwest China: application to lake basin evolution, Int. J. Coal Geol. 168 (2016) 20–34, https://doi.org/10.1016/j.coal.2016.06.003.
[30] A. Liu, R. Bechtel, R.F. Sachsenhofer, D. Gross, R. Gratzer, X. Chen, Depositional environment of oil shale within the second member of permian lucaogou formation in the Santanghu Basin, Northwest China, Int. J. Coal Geol. 175 (2017) 10–25, https://doi.org/10.1016/j.coal.2017.02.008.
[31] Y.S. Pan, Z.L. Huang, T.J. Li, X.B. Guo, X. Chen, Environmental response to volcanic activity and its effect on OM enrichment in the Permian Lucaogou formation of the Malang Sag, Santanghu Basin, Northwest China, Palaeogeogr. Palaeoclimatol. Palaeoecol. 560 (2020) 110024, https://doi.org/10.1016/j.palaeo.2020.110024.
[32] M. Yu, G. Gao, M. Liu, H. Liang, J.-L. Kang, X.-F. Xu, X.-Y. Zhao, Sedimentary environment shift and organic matter enrichment mechanism in response to volcanic ash influence: a case study of the Permian Lucaogou Formation, Santanghu Basin, NW China, J. Palaeogeogr. (2024), https://doi.org/10.1016/j.jop.2024.07.003.
[33] H. Liang, X.N. Li, Q. Ma, H. Liang, Q.S. Luo, X. Chen, G.J. Bai, Q. Zhang, Y.L. Meng, Geological features and exploration potential of permian tiaohu formation tight oil, Santanghu Basin, NW China, Pet. Explor. Dev. 41 (05) (2014) 563–572.
[34] X.F. Xu, X.C. Yu, Z. Qing, Y.T. Zhang, T.J. Li, H.Y. Yu, B.Q. Wang, Lithofacies characteristics and its relationship with shale oil reservoirs of lucaogou formation in Santanghu Basin, Xinjiang, Pet. Geol. 41 (06) (2020) 677–684.
[35] T.G. Fan, X.F. Xu, L. Fan, Y.Q. Feng, W.H. Liu, J.T. Liu, M.Y. Wang, G.Q. Jia, Geological characteristics and exploration prospect of shale oil in permian lucaogou formation, Santanghu Basin, China Pet. Explor 26 (04) (2021) 125–136.
[36] S.J. Liang, Z.L. Huang, B. Liu, L.C. Yan, H.M. Li, J. Ma, Formation mechanism and enrichment conditions of lucaogou formation shale oil from malang sag, santanghu Basin, Acta Pet. Sin. 33 (04) (2012) 588–594.
[37] S.H. Zhang, C.Y. Liu, H. Liang, L.B. Jia, J.K. Bai, L. Zhang, J.Q. Wang, Mineralogical composition and OM characteristics of lacustrine fine-grained volcanic-hydrothermal sedimentary rocks: a data-driven analytics for the second member of Permian Lucaogou Formation, Santanghu Basin, NW China, Mar. Pet. Geol. (2021) 104920, https://doi.org/10.1016/j.marpetgeo.2021.104920.
[38] X. Fang, C.G. Hao, J.T. Liu, W. Song, Geological conditions and enrichment factors of the lucaogou formation diamictite tight oil in Santanghu Basin, Xinjiang, Geol. Bull. China 42 (Z1) (2023) 397–410.
[39] S.J. Liang, Q.S. Luo, R. Wang, X. Chen, B. Yang, Q. Ma, H. Liang, Geological characteristics and exploration practice of unconventional Permian oil resources in the Santanghu Basin, China, Pet. Explor 24 (05) (2019) 624–635.
[40] J.Y. Guo, N.N. Zhong, H. Liang, X. Li, D.L. Wang, W. Ma, H.Y. Cui, Study on the source and distribution of Middle Permian oils in the Santanghu Basin, Geochimica 41 (03) (2012) 266–277.
[41] S. Tao, Y.B. Xu, D.Z. Tang, H. Xu, S. Li, S.D. Chen, W.B. Liu, Y. Cui, M.F. Gou, Geochemistry of the Shitoumei oil shale in the Santanghu Basin, Northwest China: implications for paleoclimate conditions, weathering, provenance, and tectonic setting, Int. J. Coal Geol. 184 (2017) 42–56, https://doi.org/10.1016/j.coal.2017.10.008.
[42] B. Liu, Y.F. Lv, R. Zhao, X.X. Tu, X.B. Guo, Y. Shen, Formation overpressure and shale oil enrichment in the shale system of Lucaogou Formation, Malang Sag, Santanghu Basin, NW China, Pet. Explor. Dev. 39 (06) (2012) 699–705.
[43] J. Ma, Z.L. Huang, Z.Z. Liu, C.C. Chen, X.Y. Gao, Tight reservoir characteristics of sedimentary organic matter-bearing tuff in Tiaohu Formation of Santanghu Basin, Earth Sci. Front. 22 (06) (2015) 185–196.
[44] C.G. Wang, B. Yang, Oil and gas exploration prospect in Santanghu Basin, Xinjiang. Pet. Geol. 2 (2002) 92–94+82.
[45] X.B. Guo, L.F. Zhou, Y.S. Pan, Z.L. Huang, X. Chen, S.C. Mu, C.L. Zhang, Pore structure and oil-bearing property of laminated and massive shale of Lucaogou Formation in Malang Sag, St. Basin Geol. J. 59 (3) (2023) 980–999, https://doi.org/10.1002/gj.4553.
[46] G.W. Zhang, S. Tao, D.Z. Tang, Y.B. Xu, Y. Cui, Q. Wang, Geochemical characteristics of trace elements and rare earth elements in Permian Lucaogou oil shale, Santanghu Basin, J. China Coal Soc. 42 (08) (2017) 2081–2089.
[47] A.S. Pepper, P.J. Corvi, Simple kinetic models of petroleum formation. Part I: oil and gas generation from Kerogen, Mar. Pet. Geol. 12 (1995) 291–319, https://doi.org/10.1016/0264-8172(95)96975-9.
[48] D.W. Houseknecht, D.O. Hayba, Modeling oil generation in the undeformed part of the Arctic national wildlife refuge, 1002 area. U.S. Geol, Surv 98 (1998) 1–24.
[49] Y.Y. Ma, T.T. Cao, L. Snowdon, M.H. Qian, Q.G. Jiang, M.W. Li, N. Mahlstedt, B. Horsfield, Impact of different experimental heating rates on calculated hydrocarbon generation kinetics, Energy Fuels 31 (10) (2017) 10378–10392, https://doi.org/10.1021/acs.energyfuels.7b02024.
[50] S. Bhullar, S. İnan, T.Y. Qathami, İnan, Artificial maturation of a Silurian hydrocarbon source rock: effect of sample grain size and pyrolysis heating rate on oil generation and expulsion efficiency, Int. J. Coal Geol. 285 (2024) 104475, https://doi.org/10.1016/j.coal.2023.104475.
[51] S.J. Liu, G. Gao, W.Z. Gang, B.L. Xiang, M. Wang, Differences in geochemistry and hydrocarbon generation of source-rock samples dominated by telalginite and lamalginite: a case study on the Permian saline lacustrine source rocks in the Jimusaer Sag, NW China, Pet. Sci. 20 (1) (2023) 141–160, https://doi.org/10.1016/j.petsci.2022.12.006.
[52] W. Yuan, G.D. Liu, L.M. Xu, X.B. Niu, Main controlling factors of organic matter enrichment in the Chang 7 Member of the Ordos Basin. Oil & Gas, Geology 40 (02) (2019) 326–334.
[53] R.H. Zheng, Z.P. Li, W.R. Zeng, Q.L. Yu, K.X. Man, W. Xiao, Z.H. Zhang, Distribution of hydrocarbon generation activation energy in the Chang 7 Member of the Ordos Basin and its implications for in-situ transformation of shale, Acta Geol. Sin. 97 (01) (2023) 197–209, https://doi.org/10.19762/j.cnki.dizhixuebao.2022230.
[54] P. Shetty, M.M. Gitau, G. Maróti, Salinity stress responses and adaptation mechanisms in eukaryotic green microalgae, Cells 8 (2019) 1657, https://doi.org/10.3390/cells8121657.
[55] Z. Zahra, D.H. Choo, H. Lee, A. Parveen, Cyanobacteria: review of current potentials and applications, Environ 7 (2020) 13, https://doi.org/10.3390/environments7020013.
[56] D.S. Domozych, M. Ciancia, J.U. Fangel, M.D. Mikkelsen, P. Ulvskov, W.G. T. Willats, The cell walls of green algae: a journey through evolution and diversity, Front. Plant Sci. 3 (2012) 82, https://doi.org/10.3389/fpls.2012.00082.
[57] J.S. Singh, A. Kumar, A.N. Rai, D.P. Singh, Cyanobacteria: a precious bio-resource in agriculture, ecosystem, and environmental sustainability, Front. Microbiol. 7 (2016) 529, https://doi.org/10.3389/fmicb.2016.00529.
[58] A.M. Mehdizadeh, H. Peerhossaini, Cyanobacteria: model microorganisms and beyond, Microorganisms 10 (2022) 696, https://doi.org/10.3390/microorganisms10040696.
[59] M. Manisha, Cyanobacteria: occurrence, morphology, and cell structure, Biol. Discuss. 12 (3) (2024) 123–130.
[60] J.L. Liu, D.X. Zhang, L. Hong, Isolation, characterization, and functional annotation of the salt tolerance genes through screening the high-quality cDNA library of the halophytic green alga Dunaliella salina (Chlorophyta), Ann. Microbiol. (2014), https://doi.org/10.1007/s13213-014-0967-z.
[61] H.J. Yang, J. Zhang, H. Li, Strategies of NaCl tolerance in saline-alkali-tolerant green microalga monoraphidium dybowskii LB50, Plants 12 (2023) 3495, https://doi.org/10.3390/plants12193495.
[62] R.L. Félix, M. Vicente, N. Natalia, A.E. Mari, E. Enrique, Septal protein SepJ from the heterocyst-forming cyanobacterium Anabaena forms multimers and interacts with peptidoglycan, FEBS Open Bio 7 (10) (2017) 1515–1526, https://doi.org/10.1002/2211-5463.12382.
[63] C.S. Buisan, M.N. Morión, S. Arévalo, R.F. Helm, E. Sevilla, I. Luque, M.F. Fillat, FurC (PerR) contributes to the regulation of peptidoglycan remodeling and intercellular molecular transfer in the cyanobacterium Anabaena sp. strain PCC 7120, mBio (2024) e0323123.
[64] R. Prashant, A. Singh, A.P. Gupta, J. Singh, R.P. Jaiswal, S. Sinha, Effects of ultraviolet radiation on cellular functions of the cyanobacterium Synechocystis sp. PCC 6803 and its recovery under photosynthetically active radiation, J. Photochem. Photobiol. B: Biol. 252 (2024) 112866, https://doi.org/10.1016/j.jphotobiol.2023.112866.
[65] M.D. Lewan, Evaluation of petroleum generation by hydrous pyrolysis experimentation, Org. Geochem. 39 (2) (2008) 260–283, https://doi.org/10.1016/j.orggeochem.2007.11.003.
[66] H.B. Tian, Z.X. Jiang, S. Zhang, L.Y. Shao, Characteristics and distribution of lacustrine shale oil in the upper triassic yanchang formation, Ordos Basin, China, AAPG Bull. 92 (4) (2008) 503–523, https://doi.org/10.1306/12170707116.
[67] K. He, W.J. Zhao, T. Zhang, D. Liang, L. Dai, Experimental study on the thermal cracking of crude oil and its influence on gas generation and carbon isotope fractionation, Energy Fuels 33 (5) (2019) 3977–3988, https://doi.org/10.1021/acs.energyfuels.9b00351.
[68] J. Mi, L. Shao, P. Zhang, Z.F. Feng, X. Wang, S. He, J. Zhang, Sedimentary environment and shale oil potential of the triassic yanchang formation in the Ordos Basin, China, Mar. Pet. Geol. 97 (2018) 61–78, https://doi.org/10.1016/j.marpetgeo.2018.06.004.
[69] S.F. Lu, X.T. Fu, X. Chen, J.Y. Qu, S.Y. Xue, Chemical kinetics model and calibration of gas formation from crude oil fractions, Acta Geol. Sin. 04 (1997) 367–373.
[70] W.Y. Zhang, Q. Li, Y.F. Li, S.B. Dong, S. Peng, G. Chen, Viscosity reduction and mechanism of aquathermolysis of heavy oil co-catalyzed by bentonite and transition metal complexes, Catalysts 12 (2022) 1383, https://doi.org/10.3390/catal12111383.
[71] E.E.B. Cruz, N.V.G. Rivas, U.P. García, A.M. Martinez, J.A.M. Banda, Characterization of Crude Oils and the Precipitated Asphaltenes Fraction using UV Spectroscopy, Dynamic Light Scattering, and Microscopy. InTech (2018). https://doi.org/10.5772/intechopen.70108.
[72] T.E. Ruble, M.D. Lewan, R.P. Philp, New insights on the Green River petroleum system in the Uinta basin from hydrous-pyrolysis experiments: Reply, AAPG Bull. 87 (9) (2003) 1535–1541, https://doi.org/10.1306/052803870315.
[73] Q.B. He, S.J. Chen, J. Wang, L.P. Zhao, Z.W. Ma, Geochemical characteristics and origin of crude oil from carboniferous volcanic rocks in the hongche fault zone of the junggar Basin, China, Front. Earth Sci. 10 (2022), https://doi.org/10.3389/feart.2022.870642.
[74] Y. Li, D.J. Hou, X. Cheng, X. Han, C.K. Niu, Geochemical characteristics and significance of aromatic hydrocarbons in crude oil from the East Fukang Sag, Junggar Basin, NW China, Front. Earth Sci. (2023), https://doi.org/10.3389/feart.2023.1050315.
[75] Y.X. Gan, H.J. Zhao, Z.Y. Wang, Y. Jin, W.B. Wen, J. Wang, F. Liu, X.H. Wang, G. F. Xu, Controlling factors of β-carotene enrichment in source rocks of the lucaogou formation, Malang Sag, Santanghu Basin, Acta Sedimentol. Sin. (2023) 1–18.
[76] Y. Fu, Z.D. Wang, T. Zhang, W.J. Wang, X.B. Li, Z.Y. Wang, Detection of carotenoid-like compounds in source rocks and their geological significance—a case study of well Ma-Lu 1 in the lucaogou formation, Santanghu Basin, Acta Sedimentol. Sin. (2024) 1–20.

[77] W.Q. Wang, A. Rahman, H.B. Ding, Y.J. Qiu, Assessment of aging impact on wax crystallization in selected asphalt binders, Mater 15 (2022) 8248, https://doi.org/10.3390/ma15228248.
[78] R.K. Chai, Y.T. Liu, Y.T. He, Change and mechanism of crude oil components during water flooding process. Pet, Sci. Bull. 6 (01) (2021) 114–126.
[79] L. Shi, B.J. Fan, Z.H. Li, Z.W. Yu, Z.J. Lin, X.Y. Dai, Migration differentiation of hydrocarbon components in the 7th member of triassic yanchang formation in the central Ordos Basin, Pet. Nat. Gas. Geol. 45 (01) (2024) 157–168.
[80] X. Chen, X.Q. Liu, X.C. Wang, Q. Ma, J.T. Liu, X. Gong, X.D. Yang, J.F. Shi, G.J. Bai, Formation mechanism and distribution characteristics of shale oil reservoirs in Lucaogou Formation, Santanghu Basin, Nat. Gas. Geosci. 30 (08) (2019) 1180–1189.
[81] A.Q. Tian, S. Chen, Y.X. Yu, J.L. Xiu, F. Jin, Characteristics and formation mechanism of strike-slip fault stratified deformation at the western margin of Mosuowan Uplift, Junggar Basin, Mod. Geol. 37 (02) (2023) 296–306.
[82] Z.L. Huang, J. Ma, H.Z. Wu, X. Chen, C.J. Wen, J.B. Zhang, Fluid pressure and primary migration characteristics of shale oil in Lucaogou Formation, Malang Sag. J. China Univ. Pet. (Nat. Sci. Ed.) 36 (05) (2012) 7–11+19.
[83] Z.L. Ma, L.J. Zheng, Z.X. Zhao, Y. Ge, Q. Xu, Effect of pore fluid medium on primary migration of petroleum in source rocks, Pet. Geol. Exp. 37 (01) (2015) 97–101+108.
[84] Y.B. Xu, F. Li, J.Q. Zhang, C.Q. Bi, P.C. Sun, Y.S. Shan, T. Wang, Enrichment characteristics of OM in the permian lucaogou formation in shitoumei area, Santanghu Basin, Acta Geol. Sin. 96 (11) (2022) 4010–4022, https://doi.org/10.19762/j.cnki.dizhixuebao.2022280.